Influence of sticking coefficients on the behavior of sputtered atoms in an argon glow discharge: Modeling and comparison with experiment

A. Bogaerts[a)]
Department of Chemistry, University of Antwerp, B-2610 Wilrijk-Antwerp, Belgium

J. Naylor, M. Hatcher, W. J. Jones, and R. Mason
Department of Chemistry, University of Wales Swansea, Swansea SA2 8PP, United Kingdom

(Received 19 September 1997; accepted 27 February 1998)

Two-dimensional sputtered lithium atom density profiles have been calculated with a model for an argon glow discharge. Since the value of the sticking coefficient of sputtered atoms at the cell walls, which is needed as the boundary condition for calculating the behavior of the sputtered atoms, is not available from the literature, the calculations were performed for a range of sticking coefficient values. It is found that this parameter has a significant effect on the calculation results, and accurate knowledge of its value would therefore be required for an exact description of the behavior of sputtered atoms in a glow discharge. The density profiles calculated have also been compared with experimental results, obtained with concentration-modulated absorption spectrometry at the same discharge conditions and in the same cell geometry, in order to try to make reasonable estimates for the sticking coefficients. © *1998 American Vacuum Society.* [S0734-2101(98)05704-2]

I. INTRODUCTION

Glow discharges are used in a large number of applications, e.g., in the microelectronics industry (for thin film deposition, plasma etching, and modification of surfaces), as metal vapor ion lasers, in plasma display panel technology, and in light industry. They also find application in analytical chemistry, mainly as sources for mass spectrometry and optical emission techniques, and are used for the elemental analysis of solid (mostly conducting) materials.

In the latter application, argon is mostly used as the discharge gas at a pressure of the order of 0.5–5 Torr. The discharge voltage is typically 500–1000 V and the current ranges from 1 to 50 mA. Key here is that the cathode of the glow discharge is constructed out of the material to be analyzed (mostly in the form of a disk). The cathode is bombarded by fast plasma species (mainly argon ions and fast argon atoms) that can penetrate into the cathode material. A series of collisions between the bombarding species and the atoms of the cathode material can lead to escape of the latter from the cathode if the energy they gain in such collisions is larger than their surface binding energy. This is called sputtering. The sputtered atoms arrive in the glow discharge plasma; hence, the plasma can be seen as an atom reservoir with a composition characteristic of the material to be analyzed. Suppose that a copper disk that contains impurities in concentrations of about 10^{-6} compared to the matrix element (i.e., copper; concentration of $\sim 100\%$) has to be analyzed. Then, atoms of both the matrix element and the impurities will arrive in the plasma, and the impurity atoms will have concentrations in the plasma of about 10^{-6} of the copper atom concentration. The sputtered atoms can be directly probed by an external light source, making glow discharge atomic absorption spectrometry (GD-AAS) and GD atomic fluorescence spectrometry (GD-AFS) possible.

The sputtered atoms are also subject to collisions in the plasma and they can be ionized or excited. Ions formed in this way can be measured with a mass spectrometer, leading to GD mass spectrometry (GDMS), whereas the photons created by the excitation (and subsequent de-excitation) processes can be detected by an optical spectrometer, yielding GD optical emission spectrometry (GD-OES). These two techniques (GDMS and GD-OES) comprise the majority of the analytical applications of glow discharges. From the ion peak ratio of impurity ion compared to the matrix ion (in the case of GDMS), or from the intensity ratio of optical emission spectral lines of the impurity element versus the matrix element (in the case of GD-OES), the concentration of the impurity atom versus the matrix atom in the plasma is derived, and hence also in the material to be analyzed. GDMS is most suitable for ultratrace analysis (concentrations of parts per billion) of high purity metals and alloys. GD-OES is used for trace analysis (concentrations of parts per million) of metals and alloys, e.g., in the steel industry, and especially for depth profiling of these samples (i.e., since the cathode material is more or less sputtered layer by layer, concentrations can be obtained as a function of depth in the sample).

For good analytical practice, a clear understanding of the fundamental processes taking place in the glow discharge is desirable. This can be obtained by mathematical modeling and by plasma diagnostic measurements of characteristic plasma quantities. In the last few years, a comprehensive modeling network for the various plasma species present in a glow discharge in argon has been developed by Bogaerts and co-workers (see, for example, Refs. 1–7). In Refs. 2, 5, and 7 special attention was paid to the behavior of the sputtered atoms, which is of major analytical interest.

To describe the behavior of these sputtered atoms, accurate knowledge about what happens at the walls of the discharge cell is required. However, data about sticking coeffi-

[a)]Corresponding author; electronic mail: bogaerts@uia.ua.ac.be

cients of these sputtered atoms (i.e., mostly metallic atoms) at near thermal energies are very difficult to find in the literature. The data available are for gas molecules, like H_2, N_2, rare gases (e.g., those discussed in Refs. 8–10), but not for metallic atoms, which are normally not in the gas phase, and most data are for atoms with energies in the keV range,[10] and not at thermal energies like we are interested in. Moreover, the glow discharge used for analytical applications operates under relatively high pressure conditions ($\sim$1 Torr), whereas most previous studies specifically designed to observe this sticking phenomenon are carried out under "clean" conditions and high vacuum. In Ref. 11 the sticking coefficients of a potassium beam on several target materials in a vacuum chamber were measured. These values, together with some previously published data for several beam-target combinations,[12] were used to derive some empirical relations among sticking coefficients, binding energies, and heats of formation. It was suggested that a linear relationship exists between the sticking coefficient and the binding energy of the beam target. Sticking coefficient values, ranging between <0.01 and 1.0, were tabulated for a range of beam-target combinations in vacuum.[11]

A number of models for the sputtered atoms in a glow discharge uses sticking coefficients equal to 1 (i.e., all sputtered atoms are deposited at the walls).[5,13–15] However, in Ref. 16 a comparison was made between calculated and experimental sputtered atom densities, and the authors found the best agreement when using sticking coefficients for copper atoms between 0.02 and 0.05. Bogaerts *et al.* measured sputtered tantalum atom densities by laser induced fluorescence spectrometry and by atomic absorption spectrometry, and the best correlation with their modeling results was obtained when a sticking coefficient of 0.5 was used.[17]

Because the actual value of the sticking coefficients for thermal metal atoms at typical glow discharge pressures is not known, and because these data can have large effects on the calculated sputtered atom densities (see, e.g., Ref. 7), the present work focuses on an explicit investigation of the influence of the sticking coefficients on the behavior of the sputtered atoms. Moreover, direct comparison is made with experimental observations for the same cell geometry and discharge conditions in order to estimate the values for the sticking coefficients at these particular conditions. In Sec. II, a short description of the modeling work will be given, whereas in Sec. III the experimental setup will be discussed. Results will be presented and discussed in Sec. IV, and finally, the conclusion will be given in Sec. V.

II. DESCRIPTION OF THE MODELING WORK

A comprehensive modeling network, consisting of different submodels for the various species present in the argon glow discharge, has already been developed.[1–7] A detailed description of these models will not be repeated here, but a brief summary will be given. The species assumed to be present in the glow discharge plasma include the argon gas atoms at rest, uniformly distributed throughout the discharge, argon ions and fast argon atoms, argon atoms in different excited states including metastable levels, electrons, and sputtered atoms and ions. These species are described with either a Monte Carlo model or a fluid model.

The electrons are treated with a Monte Carlo model; the collision processes incorporated are elastic collisions with argon atoms, electron impact excitation, de-excitation and ionization from the argon atom ground state and various argon atomic excited levels, electron impact ionization of the sputtered atoms, electron–argon ion recombination, and electron–electron Coulomb scattering. Moreover, the behavior of thermal electrons is also calculated in a fluid model, together with the behavior of the argon ions; the continuity and transport (by diffusion and migration) equations of electrons and argon ions are coupled to the Poisson equation to obtain self-consistent electric field distributions. In addition, the argon ions are described with a Monte Carlo model in the cathode dark space (CDS, i.e., the region adjacent to the cathode, characterized by a strong electric field), as are the fast argon atoms which are created by elastic scattering and charge transfer collisions from the argon ions. The collision processes taken into account are symmetric charge transfer for the argon ions, elastic scattering collisions for both argon ions and fast atoms, and fast argon ion and atom impact excitation, and de-excitation and ionization from the argon atom ground state and various excited levels. The argon atomic excited levels are handled with a collisional-radiative model: 65 levels are considered, and the relevant processes include electron, argon ion, fast and thermal argon atom impact ionization, excitation and de-excitation between all levels, electron–argon ion recombination to all levels, and radiative decay between all levels. Finally, the behavior of the sputtered atoms and corresponding ions is described with a fluid model and two Monte Carlo models, which will be explained below in more detail.

The Monte Carlo models are developed in three dimensions, whereas the fluid models are only two dimensional, i.e., the three dimensions could be reduced to two dimensions (axial and radial directions) due to the cylindrical symmetry of the discharge cells under investigation. All the models are coupled to each other by the interaction processes between the various plasma species, and they are solved iteratively until final convergence is reached in order to obtain an overall picture of the glow discharge. More information about these models can be found in Refs. 1–7. In the following, the models describing the behavior of the sputtered species will be explained in more detail because it is directly relevant for the present work.

The cathode material is assumed to be pure lithium. This is not one of the most commonly encountered cathode materials for elemental analysis, but it was used here for the purpose of direct comparison with experiment. In the present experimental setup, lithium is one of the only elements with suitable lines corresponding to the available laser wavelength (see Sec. III).

The atoms of the cathode material are sputtered away due to the bombardment of the cathode by argon ions, fast argon atoms, and ions of the cathode material. The sputtered atoms

leave the cathode with energies of 5–10 eV; they lose these energies almost immediately by elastic collisions with argon gas atoms until they are thermalized, after which they diffuse further into the plasma or back towards the cathode. Since thermalization is much faster than diffusion, it can be assumed that the former is already finished when diffusion starts.[13] Both processes can therefore be separated in time when modeling the behavior of the sputtered atoms, i.e., simulation of the thermalization process results in a thermalization profile, which is used afterwards as the starting distribution in the description of the diffusion process.

The thermalization process is described with a Monte Carlo model. The sputtered atoms leave the cathode with an energy and angular distribution given by[13]

$$\Psi(E,\theta)=\frac{2UE}{(E+U)^3}\frac{\cos\theta}{\pi},$$

where U is the surface binding energy of the cathode material, taken mostly to be equal to the sublimation energy, and θ is the axial angle. The specific angle and energy of a sputtered atom starting at the cathode are calculated from the above equation using two random numbers between 0 and 1. The azimuthal angle, φ, is also determined by a random number (RN) between 0 and 1: $\varphi=2\pi$ RN. The initial axial (z) coordinate is zero, and the initial radial coordinates (x and y) are determined from the radial distribution of the fluxes of the bombarding particles. During successive time steps, the trajectory of the sputtered atoms is calculated with Newton's laws. The thermalization is caused by energy losses due to collisions. Only elastic collisions with the argon gas atoms are incorporated, because this process has the highest cross section and the density of the argon gas atoms is much higher than that of any other species in the plasma. The probability of such a collision during each time step is calculated and compared to a random number. If the collision probability is lower than the random number, no collision takes place, and the atom is followed during the next time step. If the collision probability is higher, a collision takes place, and the new energy and three-dimensional direction after the collision are determined. Then, the atom is followed during the next time step and the procedure is repeated, until the atom is thermalized (i.e., when its energy has become lower than about 0.05 eV). By following a large number of sputtered atoms in this way, the thermalization profile can be obtained. More details about this Monte Carlo model can be found in Ref. 2.

The further transport of the sputtered, thermalized atoms is determined by diffusion. Moreover, these atoms can be ionized, leading to the formation of ions of the cathode material. The behavior of the sputtered atoms and the corresponding ions is described with a fluid model including the following equations:

$$\frac{\partial n_{\mathrm{Li}}(z,r)}{\partial t}+\nabla.\overline{j_{\mathrm{Li}}}(z,r)=R_{\mathrm{prod,Li}}(z,r)-R_{\mathrm{loss,Li}}(z,r), \quad (1)$$

$$\frac{\partial n_{\mathrm{Li}^+}(z,r)}{\partial t}+\nabla.\overline{j_{\mathrm{Li}^+}}(z,r)=R_{\mathrm{prod,Li}^+}(z,r), \quad (2)$$

$$\overline{j_{\mathrm{Li}}}(z,r)=-D_{\mathrm{Li}}\nabla n_{\mathrm{Li}}(z,r), \quad (3)$$

$$\overline{j_{\mathrm{Li}^+}}(z,r)=-D_{\mathrm{Li}^+}\nabla n_{\mathrm{Li}^+}(z,r)-\mu_{\mathrm{Li}^+}n_{\mathrm{Li}^+}(z,r)\nabla V(z,r), \quad (4)$$

$$R_{\mathrm{prod,Li}}(z,r)=J_0F_T(z,r), \quad (5)$$

$$R_{\mathrm{loss,Li}}(z,r)=R_{\mathrm{prod,Li}^+}(z,r)=n_{\mathrm{Li}}(z,r)[R_{e,\mathrm{ion}}(z,r)+k_{\mathrm{Pi}}n_{\mathrm{Ar,met}}(z,r)+k_{CT}n_{\mathrm{Ar}^+}(z,r)]. \quad (6)$$

Equations (1) and (2) present the continuity equations of cathode (lithium) atoms and ions, respectively. n_{Li} and n_{Li^+} are the densities of the lithium atoms and ions, and $\overline{j_{\mathrm{Li}}}$ and $\overline{j_{\mathrm{Li}^+}}$ are the respective fluxes [governed by diffusion for the atoms (Eq. (3) and by diffusion and migration for the ions (Eq. (4)]. D_{Li} is the diffusion coefficient of the lithium atoms in argon, which is calculated with a formula of the rigid-sphere model for a mixture of two chemical species.[18] It is assumed that diffusion is not determined by the charge of a particle, and therefore the diffusion coefficient of the lithium ions (D_{Li^+}) is taken to be equal to that of the lithium atoms, i.e., $D_{\mathrm{Li}}=D_{\mathrm{Li}^+}=182\ \mathrm{cm^2\ s^{-1}}$ at 1 Torr argon and 298 K. The mobility of the lithium ions (μ_{Li^+}) is adopted from a graph in Ref. 19 that shows the mobility as a function of the ion mass in argon, neon, and helium, and is taken to be $4092\ \mathrm{cm^2\ s^{-1}\ V^{-1}}$ at 1 Torr argon. $V(z,r)$ represents the potential distribution throughout the discharge, calculated self-consistently with our model.[3,6]

The production rate of the lithium atoms [$R_{\mathrm{prod,Li}}$; Eq. (5)] is given by the product of the thermalization profile [$F_T(z,r)$] and the sputtered flux from the cathode (J_0). $F_T(z,r)$ is computed in the Monte Carlo model of the thermalization process (see above). J_0 is calculated from an empirical formula of the sputtering yield, adopted from Ref. 20, and the flux energy distributions of the particles bombarding the cathode (i.e., the argon ions and fast atoms, and also the lithium ions):

$$J_0=-\int_E\{Y_{\mathrm{Ar-Li}}(E)[f_{\mathrm{Ar}^+}(0,E)+f_{\mathrm{Ar}}(0,E)]+Y_{\mathrm{Li-Li}}(E)f_{\mathrm{Li}^+}(0,E)\}dE,$$

where $Y_{\mathrm{Ar-Li}}(E)$ and $Y_{\mathrm{Li-Li}}(E)$ are the sputter yields of bombarding argon particles and lithium particles on a lithium cathode, respectively, as a function of the bombarding particle energies,[15] $f_{\mathrm{Ar}^+}(0,E)$, $f_{\mathrm{Ar}}(0,E)$, and $f_{\mathrm{Li}^+}(0,E)$ are the flux energy distributions of argon ions, argon atoms, and lithium ions at the cathode, respectively. The $(-)$ sign indicates that the flux of sputtered lithium atoms is in the opposite direction of the fluxes of the bombarding particles.

The loss rate of the lithium atoms ($R_{\mathrm{loss,Li}}$) is equal to the production rate of lithium ions ($R_{\mathrm{prod,Li}^+}$) and expresses the ionization of lithium atoms by electron impact ionization, Penning ionization by argon metastable atoms, and asymmetric charge transfer by argon ions [Eq. (6)]. $R_{e,\mathrm{ion}}$ is the electron impact ionization rate, calculated in the Monte Carlo model for electrons. $n_{\mathrm{Ar,met}}$ and n_{Ar^+} are the densities of ar-

gon metastable atoms and argon ions, and k_{PI} and k_{CT} are the rate coefficients of Penning ionization and asymmetric charge transfer, respectively. k_{PI} was obtained from an empirical formula of the corresponding cross section,[21] which was fitted to some experimentally obtained cross sections[21,22] in order to arrive at approximate values for other elements; a value of 3.2×10^{-10} cm^3 s^{-1} was obtained in this way. Cross sections or rate coefficient values for asymmetric charge transfer between argon ions and metal atoms are very difficult to find in the literature (see, e.g., the discussion in Ref. 23). It is generally known that this process is most likely when the energy difference between levels of the bombarding ion and the ion created is sufficiently small, and that the probability of this process decreases rapidly with an increasing difference in energy. Since lithium ions do not possess energy levels that lie closely to the argon ion energy levels, we assumed that asymmetric charge transfer between argon and lithium is not very probable, and therefore k_{CT} is taken as equal to zero.

This set of coupled differential equations is discretized into finite difference equations[24] and the resulting bitridiagonal system is solved with the extended Thomas algorithm, described in the appendix of Ref. 24. A typical time step of 10^{-6} s was used.

The boundary conditions for this system are determined by the sticking coefficients of lithium atoms and ions. For the lithium ions, both the boundary conditions $n_{Li^+}=0$ (i.e., sticking coefficient $A_{Li^+}=1$) and $\nabla n_{Li^+}=0$ (i.e., sticking coefficient $A_{Li^+}=0$) at all walls resulted in exactly the same density profiles, which indicates that the boundary conditions of Li^+ have actually no influence on the Li^+ density profiles. For the lithium atoms, however, varying the boundary conditions between $n_{Li}=0$ (i.e., $A_{Li}=1$) and $\nabla n_{Li}=0$ (i.e., $A_{Li}=0$) yielded clearly different results for the Li atom density (and hence, in this way also for the Li^+ ion density, because the ions are formed from the atoms by ionization, and their density depends, therefore, on the Li atom density). Since the actual value of the sticking coefficient is unknown, we varied this value between 1 (100% sticking) and 0.01 (1% sticking). Zero percent sticking at the walls is unrealistic because it is experimentally observed that there is always some amount of material deposition at the cell walls; moreover, if there were 0% sticking, the sputtering would continue to increase the Li density. The results will be compared with experimental sputtered atom density profiles, and the value of the sticking coefficient that yields best agreement with experiment will give us an estimate of this parameter.

Finally, a Monte Carlo model is used to describe the behavior of the lithium ions in the CDS. Indeed, the lithium ions are again accelerated towards the cathode by the strong electric field in this region, and they can also give rise to sputtering when they bombard the cathode. A Monte Carlo model is applied for this purpose in order to calculate the full flux energy distribution of the lithium ions, which is necessary to compute the amount of sputtering (see above).

The modeling network is applied to the same cell geometry that was used in the experimental setup: the anode (made of stainless steel) and the cathode (stainless steel covered with a lithium foil) are two parallel plates with diameters of 29 mm. They are placed 4.5 mm from each other [see Fig. 1(a)], and are inserted into a Pyrex glass housing (in the model, a cylinder with an internal diameter of 5 cm was assumed for the cell geometry). Since the glow discharge is confined between the two circular electrodes, the discharge region can be considered as cylindrically symmetrical, and the modeling results can be presented in two dimensions (axial and radial directions). Finally, a static argon background pressure is assumed in the model. In reality, there is some gas flow through the cell (due to gas inlet and pumping down), but it is so small that it may be neglected in the model.

III. EXPERIMENTAL SETUP

As mentioned before, the experiments were carried out using parallel plate electrodes mounted inside a Pyrex glass four-way cross (measuring 25 cm on the cross and having an internal diameter of 52 mm); see Fig. 1(a). The anode consisted of a stainless steel disk (29 mm in diameter) in a circular PTFE mold of 39 mm external diameter, with the surface faces flush. This was supported and connected by a 3 mm diam rod through a flange fitted to one of the ports. The rod was insulated by PTFE sleeving. The cathode was similar except that a lithium foil (Goodfellows, 0.25 mm thick) was stretched and clamped over the stainless disk by a PTFE push fit ring. Again the faces were flush and the diameters matched those of the anode. The cathode was supported through a flange on the opposite port.

Because of the sensitivity of lithium to air, the lithium foil was first cut to shape inside an argon glovebox and quickly transferred into an argon environment to the glow discharge apparatus, fitted, and immediately pumped down. The whole transfer operation required approximately 10 s and the surface was not noticeably affected.

The distance between the electrodes could be adjusted by sliding the supporting rod through a Cajon Ultra-torr™ adapter. The precise interelectrode distance was measured using the laser system.

Gas inlets and outlets, the pressure measurement device (baratron 0–13 Torr pressure transducer), and the thermocouple leads passed through appropriate feedthroughs in either of the flanges. The temperature of the cathode was monitored by a thermocouple embedded into a disk from the rear. Glass housing and extensive insulation were required to restrict the discharge to only the surfaces of the exposed disk electrodes.

The spectroscopic measurements were performed using concentration-modulated absorption spectroscopy (COMAS) which is described elsewhere[25,26] and hence is discussed here only briefly. It is a pump/probe laser technique. With the spectroscopic apparatus at our disposal, an argon ion laser pumps a DCM dye laser providing wavelengths tunable in the range of 620–680 nm. Lithium was chosen for study because it has a strong transition in this region at 670.8 nm and has been successfully studied by this technique before.[27]

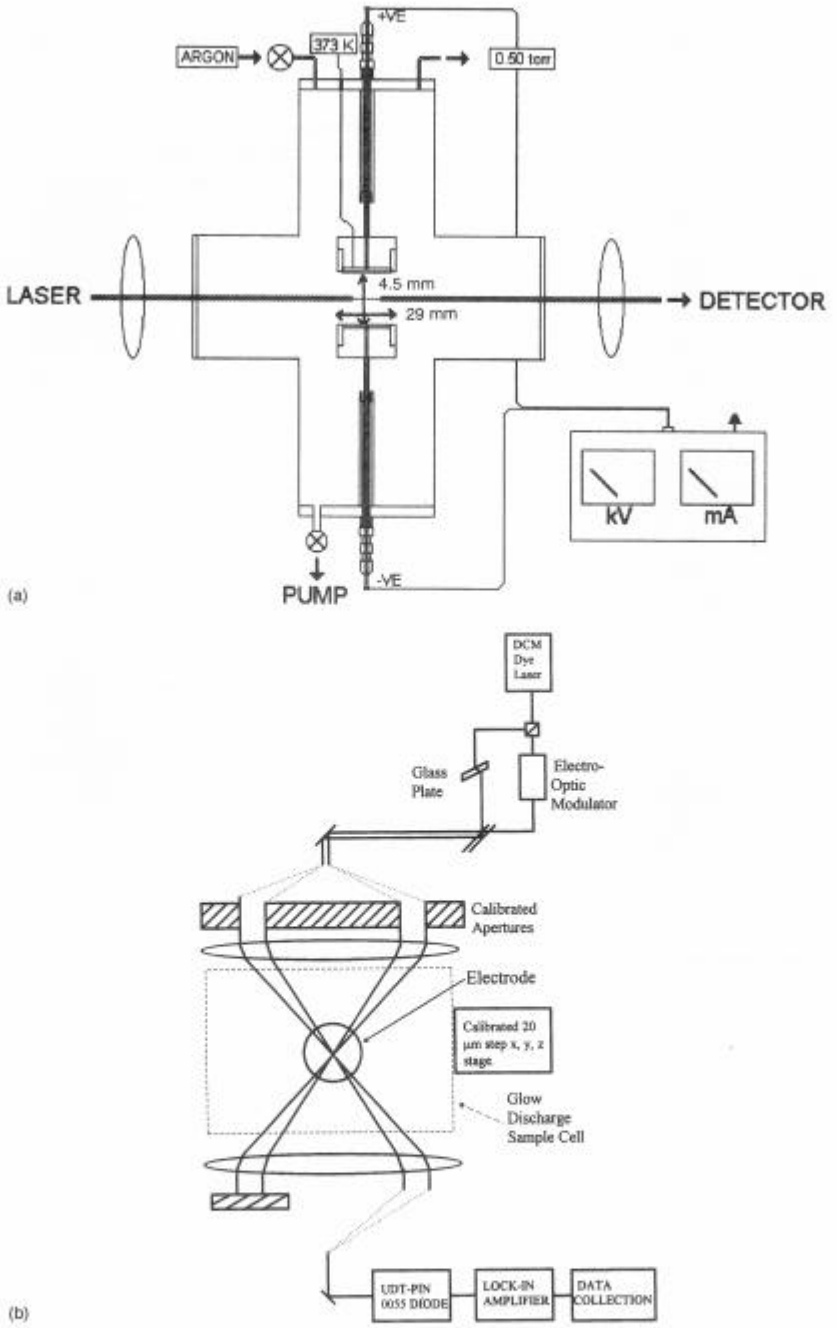

FIG. 1. Experimental setup: (a) glow discharge source and (b) COMAS laser technique.

The advantage of the COMAS method is that it allows absolute concentration measurements, within very small volumes, without the need for calibration.

To make the measurement, the beam is split into two components [see Fig. 1(b)] with out of phase polarization vectors. The pump beam is modulated at 6 MHz by a Pockel's cell and a function generator (Stanford Research Systems model DS340) and the probe beam polarization is rotated through 90° with respect to it. The probe beam signal is monitored using a photodiode (PIN-UDT 6D-0055) and a lock-in amplifier (Princeton 5202). The laser excites the lithium atoms via the $2s \rightarrow 3p$ transition. When the pump is on, the probe registers a reduced ground state population of lithium atoms, but it registers the full ground state population

when the pump is off. Hence, the probe signal has a modulated component. This modulated portion of the detector signal is called the COMAS gain, G, and it is proportional to the density of ground state atoms in the confocal volume of the cross beams. G can be measured to a precision of $\pm 1\%$.

The absolute atom density, N, is given by the following relation:[28]

$$N = \frac{2\pi i_p \ln(I_0/I)^2}{\lambda G L^2},$$

where i_p is the number of pump photons (measured to within a 0.5% precision using a Spectra-Physics laser power meter), L is the absorbance path length of the cell, λ is the transition wavelength (accurate to $<0.1\%$), and I_0/I is the inverse sample transmittance.

Keeping the experimental conditions identical to those of the COMAS gain measurements, the transmittance is measured in a separate experiment, but with the discharge treated as a standard absorption cell. For this experiment, the pump and probe beams are separated and the probe is allowed to pass through while the opposite phase pump beam passes outside the discharge but parallel to the probe, thus acting as the reference. The beams are then recombined and brought to focus at the photodiode detector. With the discharge off, the relative amplitudes are adjusted until the beams cancel each other (because they are out of phase). The probe is then temporarily blocked off to cause a signal displacement which gives the 0% transmittance level and hence a measure of I_0. When the discharge is switched on (and stabilized), the displacement gives a measure of I. In this way, the absorbance of the discharge at a specific distance from the electrodes can be measured to a precision of $\pm 1\%$.

The effective absorbance path length, L, is approximated by scanning in the y or z direction across the discharge using the COMAS method of measurement. The full atom density profile is not completely square. However, the area beneath the curve is measured and the effective path length is calculated by dividing the area by the atom density at its highest point, as if it were a square wave profile. This was done both close to the cathode where the absorbance was greatest and close to the anode where it was the least. The L values obtained were in close agreement, the average giving a precision of $\pm 0.5\%$. This needs to be done only once for each run because the linear nature of concentration to absorbance means that other gain values can be referenced to this to find true N values.

At the beginning of the experiment, the laser was tuned up on the signal in the most intense part of the discharge (close to the cathode) for fine tuning of the wavelength. The initial beam characteristics (e.g., intensity) were checked to see that they remained constant before and after measurement. The gas pressure and discharge are allowed to equilibrate for 10 min prior to any gain or absorbance measurements.

Profiling of the lithium atom densities was achieved by moving the discharge apparatus which was mounted on an Ealing Electro-optics three-way platform. Each movement was micrometer controlled to within 20 μm. All the optics therefore remained fixed. The two beams pass through crown glass windows attached to the faces of the cross perpendicular to the flanges carrying the electrodes. In the first instance, the beams were set parallel to the face of the electrodes, without a discharge running, and the interelectrode distance was measured precisely by noting the beam cutoff as the apparatus was moved in the direction perpendicular to the beam. Moving the apparatus in this way made no noticeable difference to the beam intensities and hence did not contribute to any experimental error.

The beams were crossed at an angle of 0.264°, and the confocal parameters were therefore <7.5 mm long by <0.056 mm in diameter. The confocal volume was therefore $<1.9\times10^{-5}$ cm^3 and the resolution in the xy plane <60 μm. Profiles were measured in the xy plane, perpendicular to the beam axis. The atom densities were found to be constant to within less than $\pm 2\%$ over a region within a 5 mm radius of the center of the disk. The confocal length is well within this parameter and hence gives a correct value of the atom density within this region with a better than 5% accuracy.

IV. RESULTS AND DISCUSSION

Figure 2 shows the calculated density profile of sputtered lithium atoms, in the two-dimensional cross section of the cylindrical cell geometry (z = axial direction, r = radial direction), at 444 V, 590 mTorr, and 4 mA when a sticking coefficient, A_0, of 0.05 is assumed (i.e., somewhat intermediate in the range of 0.01–1). The cathode and anode of the cell are indicated by the black thick lines at the left and right borders of Fig. 2, respectively (both with 29 mm diameters). Although the entire cell is 5 cm in diameter, the sputtered atom density is only presented in the "center" of the cell (i.e., in the region of the electrodes and slightly wider), because the region further away from the center does not give additional relevant information. Figure 2 shows only the density of thermalized sputtered atoms, i.e., resulting from the fluid model (see above). It can be seen that the density reaches a maximum at about 0.5–1 mm from the cathode, and that it decreases slightly toward the anode end wall.

In Fig. 3, the calculated density of nonthermalized sputtered lithium atoms is depicted for the same conditions as those in Fig. 2, i.e., when the lithium atoms are sputtered away, they have typical initial energies of 5–10 eV, and they are not yet immediately thermalized. It follows from Fig. 3 that most nonthermalized lithium atoms are situated close to the cathode, and that their density decreases rapidly away from the cathode as more and more atoms become thermalized. In comparing Figs. 2 and 3, it can be concluded that the contribution of nonthermalized lithium atoms is almost negligible to the total lithium atom density (i.e., the sum of thermalized and nonthermalized atoms). Indeed, we have plotted the total lithium atom density profile, and it looks identical to the thermalized atom density (and therefore, the result is not presented here).

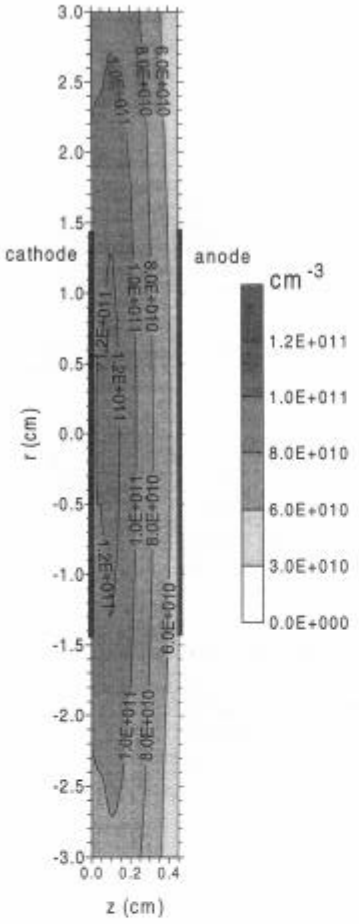

FIG. 2. Calculated two-dimensional density profile of the sputtered thermalized lithium atoms in an argon glow discharge at 444 V, 0.59 Torr, and 4 mA, assuming a sticking coefficient of $A_0 = 0.05$.

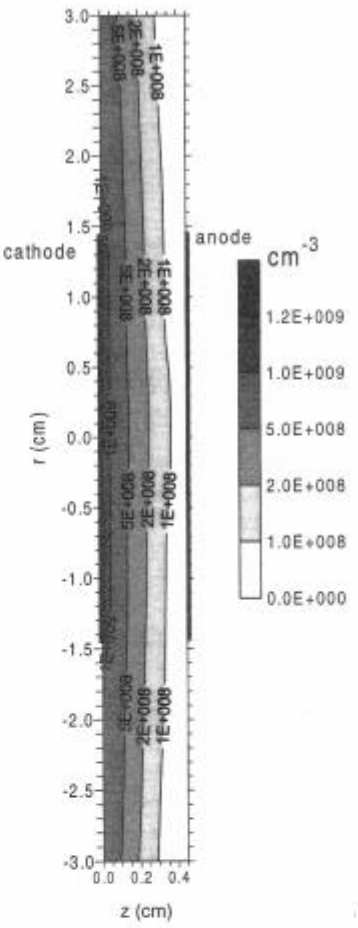

FIG. 3. Calculated two-dimensional density profile of the sputtered nonthermalized lithium atoms in an argon glow discharge at 444 V, 0.59 Torr, and 4 mA, assuming $A_0 = 0.05$.

Figures 2 and 3 show that the density is almost constant in the radial direction. The cathode and anode are only 4.5 mm apart, and this distance is much smaller than the cell diameter. We have shown before that even for a cylinder 1 cm in length and 2.5 cm in diameter, one- and two-dimensional models yielded almost the same results,[29] which illustrates that the effect of the cylinder side walls was only of minor importance. Therefore, this is certainly true for the present geometry, and the results can be presented in one dimension as well.

Figure 4 illustrates the calculated sputtered lithium atom density profiles in one dimension (i.e., the values at the cell axis) at the same discharge conditions of Fig. 2, but with sticking coefficients, A_0, ranging from 1 to 0.01. It can be seen that for a sticking coefficient of 1 the sputtered atom density has a pronounced maximum at about 1 mm and reaches zero at the cathode and anode. In fact, all the sputtered atoms remain stuck at the electrode walls (sticking probability = 100%) and therefore their density becomes zero

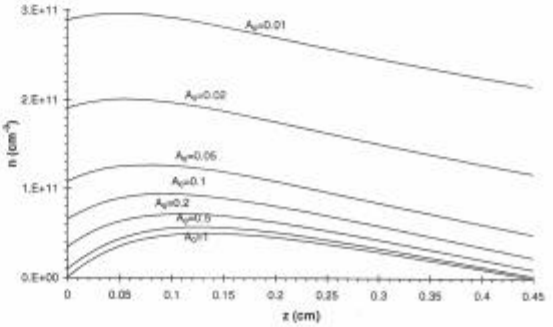

FIG. 4. Calculated sputtered lithium atom density profiles at the cell axis of an argon glow discharge at 444 V, 0.59 Torr, and 4 mA for a range of different sticking coefficients, A_0.

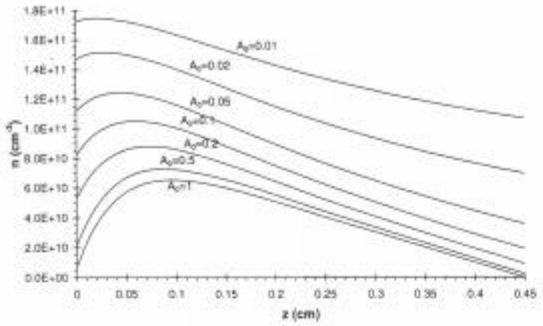

FIG. 5. Calculated sputtered lithium atom density profiles at the cell axis of an argon glow discharge at 338 V, 2.0 Torr, and 4 mA for a range of different sticking coefficients, A_0.

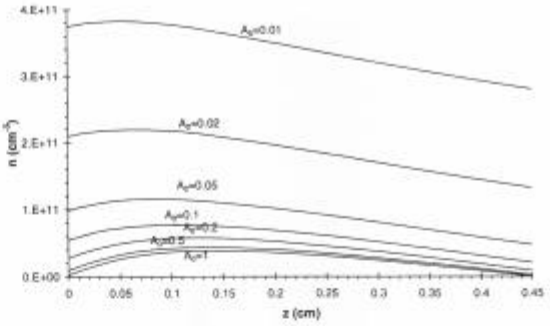

FIG. 7. Calculated sputtered lithium atom density profiles at the cell axis of an argon glow discharge at 667 V, 0.3 Torr, and 4 mA for a range of different sticking coefficients, A_0.

in the plasma adjacent to these walls. When the sticking coefficient is lowered, the absolute value of the sputtered atom density increases, the pronounced maximum about 1 mm from the cathode gradually disappears, and the density does not decrease as dramatically toward the walls anymore. The reason for this is obvious: when lowering the sticking coefficient, a smaller proportion of sputtered atoms will be removed at the walls and disappear from the plasma, so that the density in the plasma will be higher. It follows from Fig. 4 that the effect of the sticking coefficient is not linear; it is rather small when lowering the value from 1 to 0.5, and most changes are noticed at low values of A_0. Moreover, Fig. 4 clearly demonstrates that the sticking coefficient has considerable influence on the calculated density (i.e., lowering A_0 from 1 to 0.01 yields an increase in the sputtered atom density by a factor of 6). Therefore, good knowledge of this parameter is desirable in order to calculate the sputtered atom density accurately.

A similar behavior of the sticking coefficient is observed in Figs. 5–7 at the other discharge conditions investigated. The profiles were obtained for various gas pressures keeping a constant discharge current at 4 mA. This necessitated a change in the discharge voltage for each run. Figure 5 presents the results at 338 V, 2 Torr, and 4 mA; Fig. 6 shows the behavior at 383 V, 0.9 Torr, and 4 mA; Fig. 7 illustrates the effects of A_0 at 667 V, 0.3 Torr, and 4 mA. By comparing these figures, it can be seen that at high voltages and low pressures, the maximum in the profiles is not so pronounced, even at $A_0 = 1$, whereas at low voltages and high pressures, a distinct maximum is found, and the density profiles decrease more rapidly towards the end of the cell. This is attributed to the pressure effect: at high pressures, the sputtered atoms cannot diffuse so far and stay closer to the cathode, leading to a more pronounced maximum close to the cathode and a faster drop towards the end of the cell.

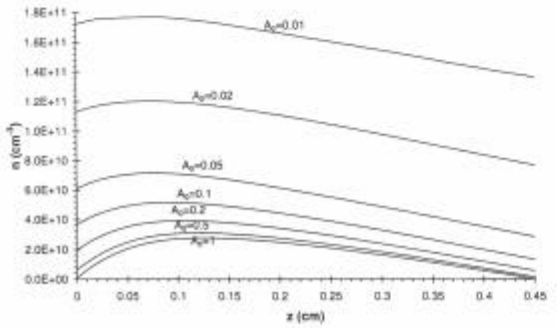

FIG. 6. Calculated sputtered lithium atom density profiles at the cell axis of an argon glow discharge at 383 V, 0.9 Torr, and 4 mA for a range of different sticking coefficients, A_0.

For comparison, experimental density profiles of sputtered lithium atoms were recorded, and the results at the four different discharge conditions investigated are illustrated in Fig. 8. In general, the shapes of the experimental profiles are in reasonable agreement with the calculation results, but the absolute values are somewhat lower (i.e., a factor of 2–10, depending on the discharge conditions and the sticking coefficients assumed). This illustrates that the model cannot yet describe the real situation exactly. This is not completely unexpected, because the empirical parameters needed to calculate the sputtering yield of lithium were not directly available in the literature[20] and some approximate values had to be adopted. The sputtering yield and the resulting sputtered atom density are therefore subject to uncertainties. On the other hand, the experiments carried out to measure these densities are also quite complicated, and the results can therefore also be subject to some errors. However, the experimental results are expected to be good to within 5%.

After all, an agreement in quantitative results within a factor of 10 is not so bad when one realizes that the modeling network does not assume certain input quantities, like fluxes bombarding the cathode to calculate the sputtering. All plasma quantities are calculated by the model itself when only pressure, voltage, and cell geometry are given, and small errors in calculated plasma quantities and in cross section data are, of course, reflected in the sputtered atom density, which is one of the final results.

It is interesting to mention here that the same model, but applied to another cell geometry, other discharge conditions, and with tantalum as sputtered cathode material (for which the sputtering yield is known in the literature with better

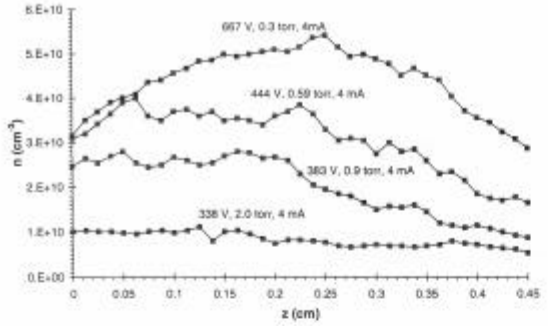

FIG. 8. Experimental sputtered lithium atom density profiles at the cell axis of an argon glow discharge at four different discharge conditions.

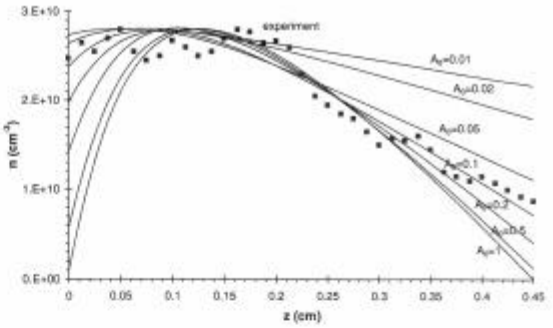

FIG. 10. Calculated sputtered lithium atom density profiles (solid lines) with different sticking coefficients at the cell axis of an argon glow discharge, normalized to the experimental density profile (black squares) at 383 V, 0.9 Torr, and 4 mA.

accuracy[20]), yielded agreement with both laser induced fluorescence (LIF) and combined LIF-atomic absorption measurements to within a factor of about 2. The calculated result was assumed to be more or less equal to the experimental values within the experimental uncertainty, because it was actually found to lie between the LIF and combined LIF-AAS results.[17]

Looking at the influence of pressure and voltage on the absolute values of the experimental density profiles, it can be concluded from Fig. 8 that the experimental density increases with decreasing pressure and increasing voltage (at constant current). This is indeed also the general trend (although less pronounced) in the calculated results. The reason for this is that at higher voltages the plasma species have higher energies upon bombardment at the cathode and they will give rise to more sputtering, since the sputtering yield increases with rising energies of the bombarding species.

Comparison of calculated and measured results can be used to define which value of the sticking coefficient leads to the best agreement between model and experiment. Based on the absolute values, the best agreement would be reached for high values of the sticking coefficient, i.e., at 338 V, 2 Torr: $A_0=1$ (even then, the calculated density is too high), at 383 V, 0.9 Torr: $A_0=1$, at 444 V, 0.59 Torr: $A_0=1$, and at 667 V, 0.3 Torr: $A_0=0.2$–0.5. However, as already mentioned before, exact quantitative agreement between calculated and experimental results cannot yet be expected, and the absolute values of the density profiles are therefore not the ideal criteria for estimating the best values for the sticking coefficients.

A better criterion is given by the relative profiles, because they are expected to be more or less correctly predicted by the model. Therefore, Figs. 9–12 show the calculated density profiles with the maximum normalized to the experimental values at the four different discharge conditions investigated. The experimental results are represented by the black squares. From Fig. 9, it follows that at 338 V, 2 Torr, and 4 mA the best agreement between model and experiment is reached for a low sticking coefficient A_0 of 0.01–0.02. At 383 V, 0.9 Torr, and 4 mA (Fig. 10), the best correspondence is found for an A_0 value between 0.02 and 0.05 at the cathode side and for A_0 equal to 0.1 at the anode side. An A_0 value equal to 0.05 seems to give the best correlation at 444 V, 0.59 Torr, and 4 mA, as seen from Fig. 11. Finally, at 667 V, 0.3 Torr, and 4 mA (Fig. 12), the closest agreement between calculated and experimental results is given for A_0 between 0.02 and 0.2. In the last case, there is some discrepancy in the relative profiles, i.e., the experimental profile

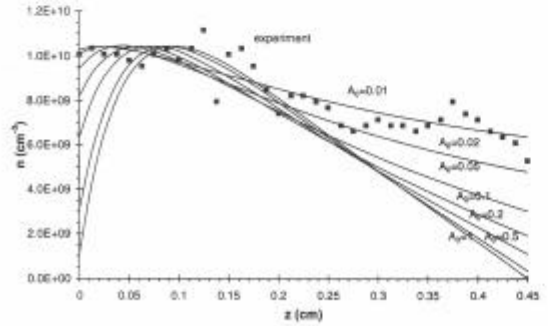

FIG. 9. Calculated sputtered lithium atom density profiles (solid lines) with different sticking coefficients at the cell axis of an argon glow discharge, normalized to the experimental density profile (black squares) at 338 V, 2.0 Torr, and 4 mA.

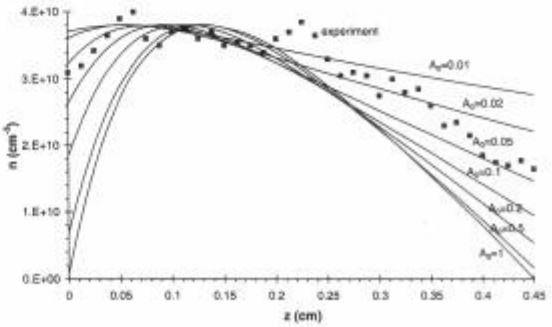

FIG. 11. Calculated sputtered lithium atom density (solid lines) profiles with different sticking coefficients at the cell axis of an argon glow discharge, normalized to the experimental density profile (black squares) at 444 V, 0.59 Torr, and 4 mA.

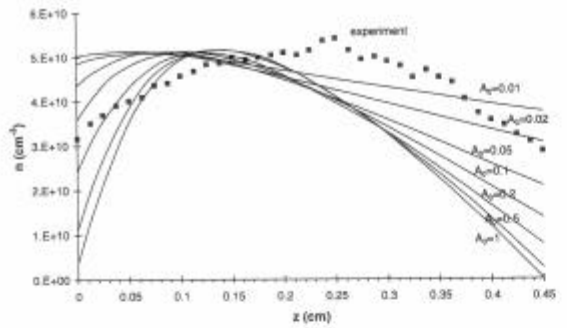

FIG. 12. Calculated sputtered lithium atom density profiles (solid lines) with different sticking coefficients at the cell axis of an argon glow discharge, normalized to the experimental density profile (black squares) at 667 V, 0.3 Torr, and 4 mA.

reaches its maximum at ~0.25 cm, whereas the calculated curves are at their maximum at about 0.1 cm. It also followed from the modeling results (Figs. 4–7) that at the lowest pressure the maximum was not so pronounced and was situated further away from the cathode (because the diffusion length of the sputtered atoms is higher at lower pressures). However, the effect seems to be much more pronounced in the experimental results, where the lowest pressure investigated yielded a maximum at 0.25 cm. This shows that complete agreement between experiment and model is not yet attained, not even in the relative profiles, and that prediction of the exact sticking coefficient values is, hence, not yet possible. Nevertheless, the results can already give a correct indication. The four discharge conditions lead to consistent results that the best agreement between model and experiment is reached for rather low values of the sticking coefficients, i.e., 0.02–0.2, decreasing slightly at increasing pressures.

The fact that the values are so low at the high pressures typical for our glow discharge is not so surprising. It indicates a competitive mechanism common for stable species in which the reactive Li atoms are competing for sites on the surface with nonactive adsorbed Ar atoms (in fact, during thin layer sputter deposition gas gets trapped). It also means that Li atoms do not automatically immediately alight upon a chemisorption site but are first physisorbed before rearranging on the surface to an energetically favored position. This is similar to the processes known to occur in reactive heterogeneous chemistry. More details on this aspect of the work (with regard to Li atoms) will be dealt with in a separate study.

Finally, it should be mentioned that the values obtained here are actually for sticking of Li atoms on a very thin layer of Li atoms already deposited on the stainless steel anode surface. Prior to that the Li atom concentration in the discharge is not completely stable (mainly due to this effect). It was also shown in Ref. 30 that after about 20 Å thickness of the adsorbate is acquired, the sticking coefficient of a beam is no longer significantly influenced by the substrate because it becomes that of the beam material sticking onto itself.

V. CONCLUSION

Sputtered lithium atom density profiles have been calculated in a glow discharge in argon at different conditions of pressure and voltage. Since the actual value of the sticking coefficient (A_0) of thermal lithium atoms is not available in the literature, the effect of this parameter on the calculated density profiles was investigated. It was found that varying this parameter has significant effect on the calculation results, i.e., lowering the value of A_0 yields higher sputtered atom densities, the effect being most pronounced at low values of A_0.

The calculated density profiles have been compared with experimental results obtained at the same discharge conditions and in the same cell geometry as assumed in the calculations in order to estimate values for the sticking coefficients. It followed that the best agreement between calculated and experimental results (based on the relative profiles) was obtained for A_0 values between 0.02 and 0.2, depending on the discharge conditions. These are rather low values in contrast to what is often assumed in modeling the behavior of the sputtered atoms (i.e., $A_0=1$). The values are, however, in good agreement with the findings of van Veldhuizen and de Hoog, who found values for copper atoms between 0.02 and 0.05.[16] For tantalum atoms, on the other hand, Bogaerts *et al.* obtained the best agreement between experiment and calculation results for $A_0=0.5$.[17] In Ref. 11 values are reported for various beam-target combinations (e.g., K, Rb, Cs, Ag, Ni, Zn,...atoms on brass, W, Al, Cu, Ag, glass,...) in vacuum ranging from <0.01 to 1.0.

This shows that the sticking coefficients do not always have the same value, and that they can vary largely, depending on the sputtered element and the surface structure of the cell walls. Moreover, the latter can change during glow discharge operation [e.g., it can become dirty due to deposition of sputtered material and/or absorption of (impurity) gas atoms] possibly leading to sticking coefficients that are not constant in time but that can change during glow discharge operation. Since this parameter seems to have a significant effect on the calculated sputtered atom densities, accurate knowledge of the sticking coefficient is required, otherwise an exact description of the behavior of the sputtered atoms in the glow discharge cannot be expected.

ACKNOWLEDGMENTS

One of the authors (A.B.) is indebted to the Flemish Fund for Scientific Research (FWO) for financial support, and she wishes to also thank the Federal Services for Scientific, Technical and Cultural Affairs (DWTC/SSTC) of the Prime Minister's office for financial support through IUAP-IV (Convention P4/10). The FWO and the British Council are also acknowledged for sponsoring the research visit of that author to the University of Wales, under the framework of the British Flemish Academic Research Collaboration Programme—1996. Finally, the same author would like to thank R. Gijbels for his continuing interest and useful discussions with respect to this work.

[1]A. Bogaerts, M. van Straaten, and R. Gijbels, Spectrochim. Acta B **50**, 179 (1995).
[2]A. Bogaerts, M. van Straaten, and R. Gijbels, J. Appl. Phys. **77**, 1868 (1995).
[3]A. Bogaerts, R. Gijbels, and W. J. Goedheer, J. Appl. Phys. **78**, 2233 (1995).
[4]A. Bogaerts and R. Gijbels, Phys. Rev. A **52**, 3743 (1995).
[5]A. Bogaerts and R. Gijbels, J. Appl. Phys. **79**, 1279 (1996).
[6]A. Bogaerts, R. Gijbels, and W. J. Goedheer, Anal. Chem. **68**, 2296 (1996).
[7]A. Bogaerts and R. Gijbels, Anal. Chem. **68**, 2676 (1996).
[8]R. T. Brackmann and W. L. Fite, J. Chem. Phys. **34**, 1572 (1961).
[9]J. N. Smith and W. L. Fite, J. Chem. Phys. **37**, 898 (1962).
[10]W. Eckstein and H. Verbeek, J. Nucl. Mater. **76 & 77**, 365 (1978).
[11]F. S. Baker and G. O. Brink, J. Chem. Phys. **37**, 1012 (1962).
[12]S. Wexler, Rev. Mod. Phys. **30**, 402 (1958).
[13]J. A. Valles-Abarca and A. Gras-Marti, J. Appl. Phys. **55**, 1370 (1984).
[14]M. van Straaten, A. Vertes, and R. Gijbels, Spectrochim. Acta B **46**, 283 (1991).
[15]M. van Straaten, R. Gijbels, and A. Vertes, Anal. Chem. **64**, 1855 (1992).
[16]E. M. van Veldhuizen and F. J. de Hoog, J. Phys. D **17**, 953 (1984).
[17]A. Bogaerts, E. Wagner, B. W. Smith, J. D. Winefordner, D. Pollmann, W. W. Harrison, and R. Gijbels, Spectrochim. Acta B **52**, 205 (1997).
[18]J. O. Hirschfelder, C. F. Curtiss, and R. B. Bird, *Molecular Theory of Gases and Liquids* (Wiley, New York, 1964).
[19]E. W. McDaniel, *Collision Phenomena in Ionized Gases* (Wiley, New York, 1964).
[20]N. Matsunami, Y. Yamamura, Y. Itikawa, N. Itoh, Y. Kazumata, S. Miyagawa, K. Morita, R. Shimizu, and H. Tawara, At. Data Nucl. Data Tables **31**, 1 (1984).
[21]L. A. Riseberg, W. F. Parks, and L. D. Schearer, Phys. Rev. A **8**, 1962 (1973).
[22]S. Inaba, T. Goto, and S. Hattori, J. Phys. Soc. Jpn. **52**, 1164 (1983).
[23]A. Bogaerts and R. Gijbels, J. Anal. At. Spectrom. **11**, 841 (1996).
[24]D. U. von Rosenberg, *Methods for the Numerical Solution of Partial Differential Equations* (Elsevier, New York, 1969).
[25]W. J. Jones, J. Chem. Soc., Faraday Trans. 2 **83**, 693 (1987).
[26]W. Mallawaarachi, A. N. Davies, R. A. Beamann, A. J. Langley, and W. J. Jones, J. Chem. Soc., Faraday Trans. 2 **83**, 707 (1987).
[27]R. M. Allott, M. Kubinyl, A. Grofcsik, W. J. Jones, and R. S. Mason, J. Chem. Soc., Faraday Trans. **91**, 1297 (1995).
[28]A. J. Langley, R. A. Beaman, A. N. Davies, and W. J. Jones, Chem. Phys. **101**, 117 (1986).
[29]A. Bogaerts and R. Gijbels, Fresenius J. Anal. Chem. **359**, 331 (1997).
[30]F. M. Devienne, J. Phys. Radium **14**, 257 (1953).